Featured Article

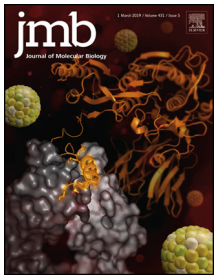

Identification of a Helical Segment within the Intrinsically Disordered Region of the PCSK9 Prodomain

M. Ultsch [1], W. Li [2], C. Eigenbrot [1], P. Di Lello [1], M.T. Lipari [2], S. Gerhardy [2], A.P. AhYoung [2], J. Quinn [3], Y. Franke [4], Y. Chen [5], M. Kong Beltran [6], A. Peterson [6] and D. Kirchhofer [2]

*1 - **Department of Structural Biology,** Genentech, Inc., 1 DNA Way, South San Francisco, CA 94080, USA*
*2 - **Department of Early Discovery Biochemistry,** Genentech, Inc., 1 DNA Way, South San Francisco, CA 94080, USA*
*3 - **Department of Biochemical and Cellular Pharmacology,** Genentech, Inc., 1 DNA Way, South San Francisco, CA 94080, USA*
*4 - **Department of Biomolecular Resources,** Genentech, Inc., 1 DNA Way, South San Francisco, CA 94080, USA*
*5 - **Department of Antibody Engineering,** Genentech, Inc., 1 DNA Way, South San Francisco, CA 94080, USA*
*6 - **Department of Molecular Biology,** Genentech, Inc., 1 DNA Way, South San Francisco, CA 94080, USA*

Correspondence to D. Kirchhofer: *dak@gene.com*
https://doi.org/10.1016/j.jmb.2018.11.025
Edited by Richard W. Kriwacki

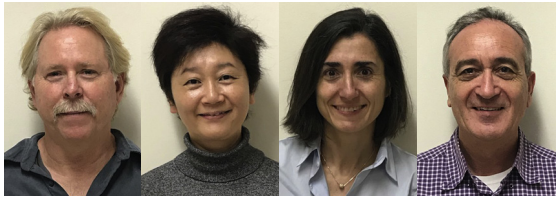

M. Ultsch, W. Li, P. Di Lello and D. Kirchhofer

Abstract

Proprotein convertase subtilisin/kexin 9 (PCSK9) is a key regulator of lipid metabolism by degrading liver LDL receptors. Structural studies have provided molecular details of PCSK9 function. However, the N-terminal acidic stretch of the PCSK9 prodomain (Q31–T60) has eluded structural investigation, since it is in a disordered state. The interest in this region is intensified by the presence of human missense mutations associated with low and high LDL-c levels (E32K, D35Y, and R46L, respectively), as well as two posttranslationally modified sites, sulfated Y38 and phosphorylated S47. Herein we show that a segment within this region undergoes disorder-to-order transition. Experiments with acidic stretch-derived peptides demonstrated that the folding is centered at the segment Y38–L45, which adopts an α-helix as determined by NMR analysis of free peptides and by X-ray crystallography of peptides in complex with antibody 6E2 (Ab6E2). In the Fab6E2–peptide complexes, the structured region features a central 2 1/4-turn α-helix and encompasses up to 2/3 of the length of the acidic stretch, including the missense mutations and posttranslationally modified sites. Experiments with helix-breaking proline substitutions in peptides and in PCSK9 protein indicated that Ab6E2 specifically recognizes the helical conformation of the acidic stretch. Therefore, the observed quantitative binding of Ab6E2 to native PCSK9 from various cell lines suggests that the disorder-to-order transition is a true feature of PCSK9 and not limited to

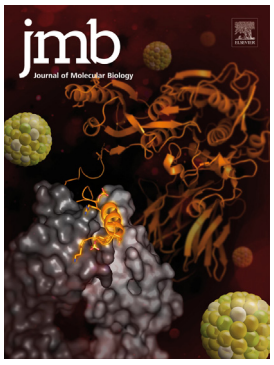

Legend: *LDL cholesterol (yellow spheres) are cleared from the blood by liver LDLRs, which in turn are regulated by circulating PCSK9 (orange ribbon model). The N-terminal region of PCSK9 harbors several missense mutations associated with high or low LDL levels, but has so far eluded structural studies, since it is intrinsically disordered. In this issue, Ultsch et al. report that upon interaction with a Fab ligand, this region becomes structured, featuring a central helix (highlighted with an orange glow). This suggests that the mutations may exert their biological functions within the context of an ordered conformational state. The amino acids depicted with side chains are the three missense mutations and the two posttranslational modification sites. Artistic illustration by Allison Bruce (A. K. Bruce Design).*

peptides. Because the helix provides a constrained spatial orientation of the missense mutations and the posttranslationally modified residues, it is probable that their biological functions take place in the context of an ordered conformational state.

Introduction

The proprotein convertase subtilisin/kexin type 9 (PCSK9) [1] is a serine protease and a member of the small family of human proprotein convertases [1,2]. The identification of gain- and loss-of-function mutations [3–6] associated with increased and decreased plasma LDL cholesterol (LDL-c) levels, respectively, established PCSK9 as an important regulator of lipid metabolism.

PCSK9 is produced as a pro-protein mainly in the liver and undergoes autocatalytic cleavage between the C-terminal residue (Q152) of the prodomain and the N-terminal residue (S153) of the catalytic domain. This processing step takes place in the endoplasmic reticulum and is a prerequisite for secretion into the blood stream [1]. Typically, proprotein convertases further degrade the prodomain to liberate enzyme activity of the catalytic domain. In contrast, the prodomain of PCSK9 is not further degraded but remains tightly bound to the active site of the catalytic domain. Instead of being an active enzyme, the mature PCSK9 now becomes a ligand for the low-density lipoprotein receptor (LDLR). This interaction is mediated by the PCSK9 catalytic domain, which binds to the epidermal growth factor-homology domain-A [EGF(A)] of LDLR in a calcium-dependent manner [7]. The EGF (A) binding site is away from the catalytic site and has a flat, slightly convex surface and includes part of the P′-helix that is formed upon auto-cleavage [8] (Suppl. Fig. S1A). An additional, albeit minor, interaction occurs between the prodomain of PCSK9 and the β-propeller region of LDLR [9] (Suppl. Fig. S1A). The binding interaction between PCSK9 and LDLR on the cell surface is regulated by heparan sulfate proteoglycans and in extrahepatic tissues by Annexin A2 [10–13]. After endocytosis, the entire PCSK9–LDLR complex is then directed to lysosomes for degradation, resulting in reduced LDLR levels. The C-terminal domain plays a critical role in this latter process, as it is indispensable for PCSK9 cellular uptake and for providing additional interactions with the LDLR to strengthen the overall affinity in the low pH endosomal compartment [9,14–18] (see Suppl. Fig. S1B for a summary of PCSK9 domain functions). Within only 12 years after the discovery of PCSK9 [2], the FDA approved two therapeutic anti-PCSK9 antibodies for clinical use. Large clinical outcomes studies in high-risk cardiovascular patient populations showed that these new therapeutics provided strong LDL-c lowering and they reduced adverse cardiovascular events [19] and, most importantly, overall mortality (ODYSSEY OUTCOMES, http://www.acc.org/latest-in-cardiology/clinical-trials/2018/03/09/08/02/odyssey-outcomes).

There are 16 PCSK9 crystal structures deposited in the Protein Data Bank (www.rcsb.org; as of July 2018), which used recombinant PCSK9 with an intact prodomain for crystallization (PDB accession codes 2P4E, 3SQO, 4NE9, 5VL7, 5VLA, 5VLH, 5VLL, 5VLP, 2PMW, 3H42, 3P5B, 3P5C, 4NMX, 5VLK, 2QTW, 4K8R). They comprise apo-structures of full length and of C-terminally truncated PCSK9 and of complexes of PCSK9 with antibody Fabs and with peptidic inhibitors. Despite the different PCSK9 forms used and the different space groups, all structures share the common feature in that there is no recognizable electron density for the N-terminal region of the PCSK9 prodomain encompassing residues Q31–T60. This strongly suggests that this segment is in a disordered state. The Q31–T60 region is also called the “acidic stretch” due to the high number of aspartic acid and glutamic acid residues (four and eight residues, respectively). The PCSK9 acidic stretch displays the hallmarks of intrinsically disordered regions (IDRs) of proteins [20,21]. This includes an enrichment of the disorder-promoting charged residues E and D, which constitute 25% of the amino acids in this segment, the presence of other disorder-promoting residues (Q, R, S, P), and the paucity of order-promoting residues (Y, L, V, H, T) [20,22], resulting in a net negative charge and low overall hydrophobicity. IDRs, such as the PCSK9 acidic stretch, constitute a large fraction of the proteome of any organism [20,21]. IDRs are frequently subject to posttranslational modifications (PTMs) that increase functionality [20,21,23,24]. In addition, they can harbor functional elements called molecular recognition features (MoRFs), which are short segments within disordered regions that undergo disorder-to-order transition upon ligand binding. These IDR features provide functional versatility in the interaction and recruitment of proteins [20,21]. A classic example is p53 [20,21], which displays a disordered N-terminal transactivation domain. A short segment within this region adopts an α-helical conformation upon interaction with its binding partner MDM2 [25–27]. Similarly, the family of the pro-apoptotic BH3-only proteins is intrinsically disordered, but their ligand-binding BH3 domains transition into an α-helix to interact with Bcl-2 family members [28,29]. This raises the possibility that,

under particular circumstances, the disordered acidic stretch of PCSK9 may also transition to an ordered state.

Consistent with the paradigm that IDRs are frequently subjected to PTMs [20,21,23,24], the disordered acidic stretch of PCSK9 contains two PTM sites, that is, sulfation of Y38 and phosphorylation of S47. Additional PTMs are glycosylation of N533 [2] and phosphorylation of the residue S688 [30,31], which is located in a region of disorder at the C-terminus, as suggested by the lack of electron density after R682 or H683 in all PDB-deposited crystal structures of PCSK9. The Y38 residue undergoes *O*-sulfation mediated by the enzyme sulfotransferase [32,33]. Interestingly, it was shown that the nearby gain-of-function mutation D35Y can also be O-sulfated [34]. The second PTM site is S47, which undergoes phosphorylation [30,31] mediated by the Golgi casein kinase FAM20C [31], and the S47-phosphorylated PCSK9 was detected in human plasma [30]. The S47 phosphorylation appears to protect the acidic stretch from proteolysis [30]. Both the Y38 and S47 residues are conserved among numerous mammalian species, suggesting that modifications of these residues may also occur in other organisms. However, it remains unknown if and how the posttranslationally modified Y38 and S47 regulate PCSK9 function *in vivo*.

Importantly, the acidic stretch harbors several missense mutations in the human population. The loss-of-function mutation R46L is associated with decreased LDL-c levels [6,35,36]. *In vitro* studies with the PCSK9–R46L mutant protein did not provide a clear explanation why this mutation lowers plasma LDL-c, since intracellular processing, secretion and LDLR function are relatively unaffected [37–40]. It was proposed that the mutation may eliminate the cleavage at the R46-S47 bond by an arginine-specific proteases such as the proprotein convertase PC7 [37]. Carriers of another missense mutation, D35Y, have highly elevated LDL-c plasma levels [34], but *in vitro* studies with this recombinantly expressed variant did not demonstrate any phenotypic changes, as its secretion, processing, and LDLR binding and degradation were similar to the wild-type protein [34]. The E32K variant [41] is located right next to the N-terminal Q31 residue. E32K carriers have higher LDL-c levels and onset of myocardial infarction occurs at a younger age compared to non-carriers [42]. This mutation seems to increase PCSK9 secretion and worsens the clinical phenotype of patients carrying additional *LDLR* mutations [43,44]. Additional genetic variants in the acidic stretch region have been identified (A53V, E54A, and E57K) but were not found to be independently associated with changes in LDL-c levels [3,6,41].

There is strong evidence that the acidic stretch is involved in binding interactions. A recent study has implicated the acidic stretch in PCSK9 binding to LDL particles, which seems to regulate the activity of PCSK9 towards LDLR [45]. Furthermore, the deletion of the acidic stretch creates a hyperactive PCSK9 displaying enhanced cellular uptake, increased potency of LDLR degradation, and stronger binding to LDLR [8,37,46]. This indicates that the acidic stretch has auto-inhibitory activity and functions as a negative regulator of PCSK9. The auto-inhibitory activity is not mediated by specific structural motifs. The acidic stretch could be shortened by a few residues, and up to six glutamic or aspartic acid residues could be charge-neutralized without changes in the auto-inhibitory activity, indicating that activity only depends on a minimal length and a minimal net charge [46]. Remarkably, the auto-inhibitory function is even independent of the amino acid sequence, since the entire stretch could be functionally substituted by an acidic, intrinsically disordered segment [47] of an unrelated protein [37]. The lack of any specific structural requirements for auto-inhibition (other than minimal length and charge) makes it difficult to explain why missense mutations having only a single amino acid change in the acidic stretch can profoundly increase or decrease plasma LDL-c levels. However, we note that concerning the R46L mutant, Benjannet *et al.* [37] mentioned a mechanism that could be associated with auto-inhibitory activity, in that the mutant's resistance to proteolysis may prevent the generation of the hyperactive PCSK9Δ46 form.

In this study, we provide evidence that a segment within the acidic stretch can undergo disorder-to-order transition. Solution NMR experiments with peptides spanning the acidic stretch region demonstrated a propensity to adopt an α-helix. This helical conformation is stabilized by binding to antibody 6E2 (Ab6E2), as demonstrated by crystal structures of Fab6E2–peptide complexes. This antibody, which specifically recognizes the helical conformation, bound to both acidic stretch-derived peptides and to intact PCSK9, suggesting that the disorder-to-order transition is a physiological property of PCSK9. Our finding that the three naturally occurring mutations and PTM sites locate to the structured region raises the possibility that these modified residues may elicit their specific functions in the context of a well-ordered helical segment.

Results

Antibody 6E2 (Ab6E2) binds to the acidic stretch of the PCSK9 prodomain

The antibody clone 6E2 was obtained by standard hybridoma technology after immunization of PCSK9 knock-out mice with recombinant human PCSK9

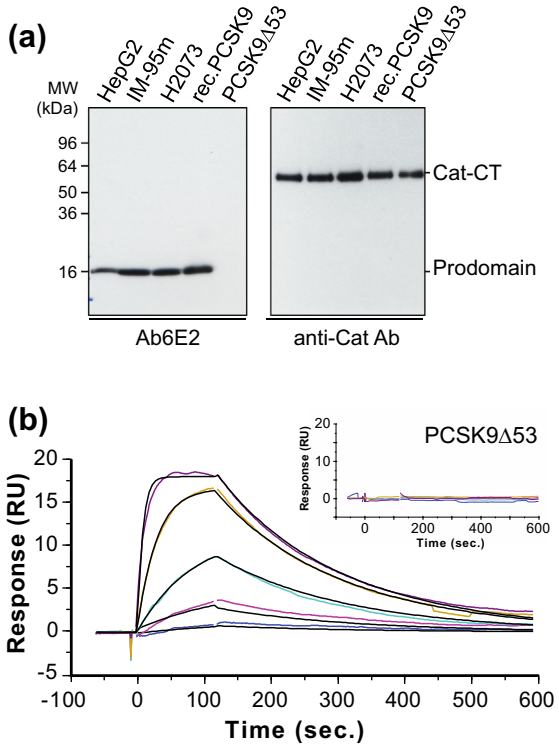

Fig. 1. Ab6E2 binds to the acidic stretch of the PCSK9 prodomain. (a) Ab6E2 detects the prodomain of recombinant PCSK9 (rec.PCSK9) and of native PCSK9 secreted by HepG2, IM-95m, and H2073 cell lines (left panel), but not the catalytic/C-terminal domain (Cat-CT), which was detected by the anti-catalytic domain antibody (anti-Cat Ab; right panel). Rec.PCSK9 lacking the acidic stretch region (PCSK9Δ53) is no longer recognized by Ab6E2. (b) Ab6E2 immobilized to a protein A sensor chip bound to rec.PCSK9 (concentration range, 1 nM–250 nM) with a K_D of 10.5 ± 1.2 nM, but did not show any detectable binding to PCSK9Δ53 up to 250 nM (inset). All figures are representative of at least three independent experiments.

(rec.PCSK9) as described [48]. The mouse IgG was reformatted into a human/mouse chimeric antibody Ab6E2 by grafting the mouse variable domains onto the human constant region of the herceptin antibody (IgG1) for expression in CHO cells. Immunoblotting experiments showed that Ab6E2 specifically detected the 16-kDa prodomain of rec.PCSK9, but not the 60-kDa band comprising the catalytic and C-terminal domain, which was detected by an anti-catalytic domain antibody (Fig. 1a). In addition, we analyzed Ab6E2 reactivity with native PCSK9 of the cancer cell lines HepG2 (hepatoma), IM-95m (gastric adenocarcinoma), and H2073 (lung adenocarcinoma). Immunoblotting of conditioned media demonstrated that Ab6E2 specifically recognized the prodomain of PCSK9 secreted by the three cell lines (Fig. 1a). Furthermore, experiments with the N-terminally truncated PCSK9, in which the acidic stretch residues Q31–A53 were deleted (PCSK9Δ53), indicated that the Ab6E2 binding site is located within the acidic stretch region. First, Ab6E2 did not detect the prodomain band of PCSK9Δ53 in immunoblotting experiments (Fig. 1a). Second, surface plasmon resonance (SPR) experiments demonstrated that Ab6E2 bound to PCSK9 with a K_D of 10.5 ± 1.2 nM, but did not interact with PCSK9Δ53 (Fig. 1b, inset).

To investigate whether the region deleted in PCSK9Δ53 (Q31–A53) contains the main antibody epitope, we synthesized a peptide corresponding to this sequence, except that the N-terminal Q31 was omitted. This peptide (Pep1) bound to Ab6E2 with a K_D value of 3.8 μM (Table 1), confirming that the antibody epitope lies within the acidic stretch. Pep1 also contains two residues subject to PTM, Y38 and S47. Therefore, peptides were synthesized containing either sulfo-Y38 (sY38; Pep2) or phospho-S47 (pS47;Pep3) or both modifications (sY38:pS47; Pep4). Remarkably, Pep2 with the sY38 modification

Table 1. Binding affinities of peptides determined by SPR

Peptide	Sequence	Changes	K_D (μM)
Pep1	^{32}EDEDGDYEELVLALRSEEDGLA^{53}	Wild-type	3.8000
Pep2	^{32}EDEDGD**sY**EELVLALRSEEDGLA^{53}	sY38	0.0019[a]
Pep3	^{32}EDEDGDYEELVLALR**pS**EEDGLA^{53}	pS47	5.0000
Pep4	^{32}EDEDGD**sY**EELVLALR**pS**EEDGLA^{53}	sY38:pS47	0.0013
Pep5	^{32}EDEDGD**A**EELVLALRSEEDGLA^{53}	Y38A	No binding
Pep6	^{32}**K**DEDGDYEELVLALRSEEDGLA^{53}	E32K	Not determined
Pep7	^{32}EDEDGDYEELVLAL**L**SEEDGLA^{53}	R46L	No binding
Pep8	^{36}DEDGDYEELMLALPSQEDGLA^{56}	Mouse	No binding
Pep9	^{32}EDE**Y**GDYEELVLALRSEEDGLA ^{53}	D35Y	Not determined
Pep10	^{32}EDEDGDYEELV**PP**LRSEEDGLA^{53}	L43P:A44P	No binding
Pep11	^{32}EDEDGDYEELV**P**ALRSEEDGLA^{53}	L43P	No binding
Pep12	^{32}EDEDGDYEELVL**P**LRSEEDGLA^{53}	A44P	No binding

K_D values were obtained by global fitting a simple 1:1 kinetic model to superimposable duplicate single cycle kinetic curves each containing five serial-tripling dose response segments.

No binding: no signal detected at 20 μM peptide concentration.

Underlined and bold: changes in respect to the wild-type sequence of Pep1.

[a] Obtained from a separate replicate assay run due to interference from air spike.

had an approximately 2000-fold increased affinity to Ab6E2 (K_D = 1.9 nM) (Table 1). In contrast, the S47 phosphorylation did not influence the binding affinity, either alone (Pep3) or in combination with the sY38 change (Pep4). The importance of the Y38 residue for binding to Ab6E2 was confirmed in SPR experiments with the Y38A mutant peptide (Pep5), which showed no measurable binding (Table 1).

The strong binding affinities of the acidic stretch-derived peptides suggested that they are good conformational mimics of this epitope region as presented in the PCSK9 protein. The interest in the conformational state of this region is heightened by the fact that, besides the two PTM sites, it also harbors missense mutations. In addition, we were curious to understand the structural basis for the strong increase in binding affinity elicited by the sulfation of the Y38 residue. Therefore, we determined the peptide conformations by use of X-ray crystallography and NMR.

Crystal structures reveal an α-helical conformation of the acidic stretch-derived peptides

The structures of the complexes of Fab6E2–Pep1 (wild-type), Fab6E2–Pep4 (sY38:pS47), and Fab6E2–Pep6 (E32K) were determined at 2.25, 2.20, and 2.10 Å resolution, respectively (see X-ray metrics in Suppl. Table S1). Overall, these complexes are remarkably similar (Fig. 2a–c). The most striking feature in all structures is a well-ordered 2 1/4-turn α-helix formed by the 9-amino-acid central portions of the peptides (^{37}DYEELVLAL^{45}). We first compare the structures of the wild-type Pep1 with Pep4, which contains the modified residue sY38 and pS47. Pep6 only differs from Pep1 by the length of the structured region and will be discussed later. The helical region of Pep1 and Pep4 shows H-bonds characteristic of α-helices from the carbonyl oxygen of G36 to the amide nitrogen of R46, and this core segment contacts Fab6E2 in almost identical ways (Fig. 2d, e). For both peptides, the N-terminal residues E32–D33–E34 are not observed in electron density and are considered disordered. Residues preceding and following the helical core are less well ordered than the helix but still present similar conformations to Fab6E2, including pS47 of the modified peptide (Pep4), which was modeled using two conformations of the side chain. Peptide residues D50–G51–L52–A53 are missing from both structures, and E49 is missing from the structure with Pep1, due to disorder. The buried solvent-accessible surface of Pep4 (~680 Å^2) is marginally larger than that of Pep1 (~610 Å^2) mainly due to the presence of sY38 and pS47 and discounting a small effect of the extra amino acid built in the Pep4 structure (E49) (Fig. 2d, e). Although the complementarity determining region (CDR) loops CDR-L1 (16 residues) and the CDR-H2 (12 residues) are relatively long [49], contacts within 4 Å of the central α-helix of the peptides (D37–L45) are restricted to residues from the CDR-H1, CDR-H3, and CDR-L2 (Fig. 2f, g). The Fab6E2 segment that differs the most between the two complexes is CDR-L1, where N28 Cα atoms, at the tip of the loop, are separated by 2.1 Å after superposition. The difference is associated with phosphorylation of S47 and coordination of a Zn^{2+} ion in the Fab6E2–Pep4 complex, which are absent in the Fab6E2–Pep1 complex as discussed below.

For both peptides, the main structural contacts with Fab6E2 consist of van der Waals (L41, V42, L45) and H-bonding interactions (Y38/sY38, E39, R46, S47, E48) originating from residues of one face of the α-helix and of three residues following the helix (R46, S47, E48) (Fig. 3a, b). The most important contacts are made by Y38/sY38, L45 and R46. The side chains of the Y38 (Pep1) and of sY38 (Pep4) are well-resolved (electron density map in Suppl. Fig. S2) and insert into a deep pocket formed by the loops of CDR-H1 and CDR-H3 with which they engage in numerous H-bonding interactions (Fig. 3c, d), explaining why the alanine replacement (Pep5) completely abolished antibody binding. These extensive interactions made by the sulfate group are consistent with the observed affinity improvement by the sY38-modified Pep2 and Pep4 (Table 1). Moreover, the structures clearly show that the affinity improvement by the sY38-modified peptides is not caused by any conformational changes but is due to the extensive interactions made by the sulfate group with a preformed pocket within the antibody paratope. This raises the question why this pocket is preformed in the Ab6E2 to allow for preferential binding to the sulfated Y38 over the non-modified form. We suspect that the recombinant PCSK9 used for immunizing PCSK9$^{-/-}$ mice may have contained some low amounts of sY38, which may have been highly immunogenic, but this remains speculative.

Structural analysis of the effect of phosphorylation of S47 is complicated by apparent disorder for the pS47 side chain and the presence in the crystallization medium of about 100 mM Zn^{2+} ions, one of which is coordinated by pS47. In our results, the pS47 side chain provides one additional H-bond *versus* Pep1's S47, the relevance of which is difficult to assess (Fig. 3e, f). This structured peptide region also contains two residues, D35 and R46, of which missense mutations have been reported to result in increased (D35Y) and decreased (R46L) LDL-c levels [6,34,35]. Residue D35 precedes the α-helix and does not contact Fab6E2 (Fig. 3a, b), whereas R46, located immediately C-terminal to the helix, is a key contact residue with Fab6E2 forming a salt bridge to CDR-H2 residue E95 and an H-bond to the main chain oxygen of CDR-H1 K31 (Fig. 3e, f). Consistent with this, replacing R46 with a leucine residue (Pep7) as found in the natural

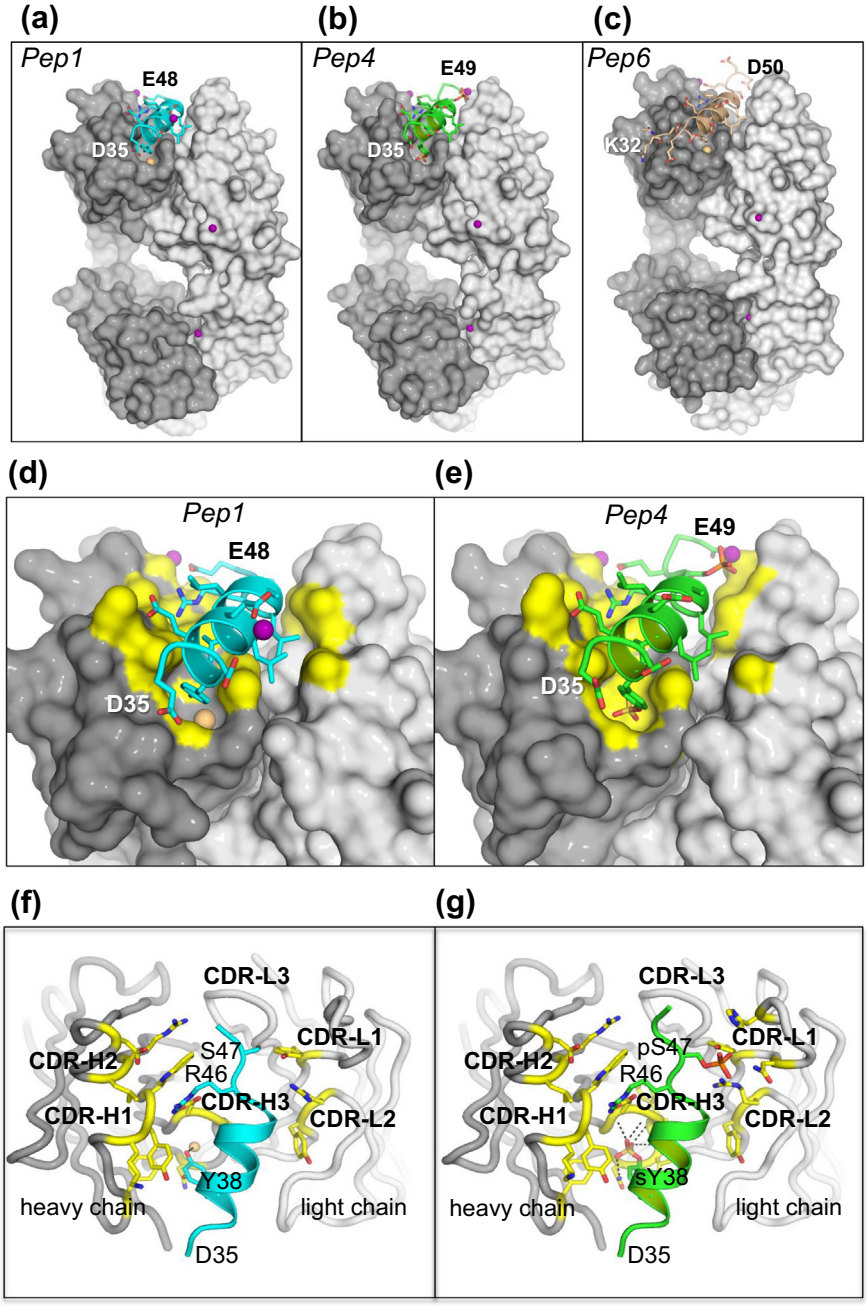

Fig. 2. Acidic stretch-derived peptides adopt an α-helical conformation in complex with Fab6E2. Fab6E2 complexes with Pep1 (wild-type), Pep4 (sY38:pS47) and Pep6 (E32K) from X-ray crystallography show substantial similarity despite different sulfation and phosphorylation status. (a–c) Overview shows Fab6E2 as surfaces (heavy chain in dark gray, light chain in light gray), with stylized peptides (a: Pep1 in cyan; b: Pep4 in green; c: Pep6 in tan). Purple spheres represent Zn^{2+} ions, and the orange sphere with Pep1 and Pep6 represents a chloride ion. The structured regions for Pep1 and Pep4 start with the N-terminal D35 and end with the C-terminal E48 in Pep1 and with E49 in Pep4. For Pep6, the structured region starts with K32 and ends with D50. (d and e) A closer view with yellow color added to the Fab surface for residues within 4 Å of the peptide. (f and g) Viewing down onto the antigen recognition site (paratope) with side chains within 4 Å of Pep1 (f) or Pep4 (g) included for Fab6E2. Three peptide amino acids preceding D35 are disordered and D35 has no distance to Fab6E2 less than 4 Å. The helical segment of both peptides has 4 Å contacts only with CDR-H1, CDR-H3, and CDR-L2. Five (Pep1) or 4 (Pep4) C-terminal amino acids are absent due to disorder.

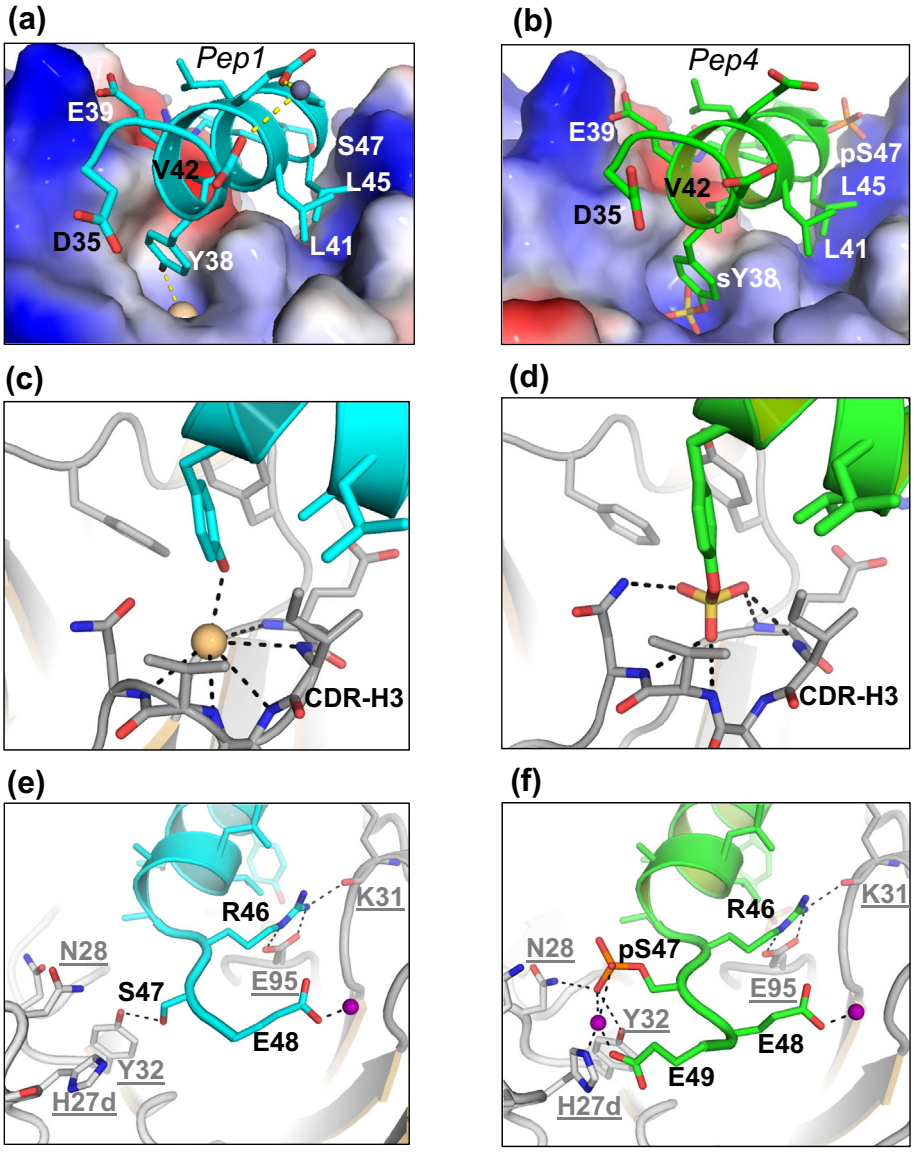

Fig. 3. Polar interactions between Fab6E2 and peptide sites subject to PTMs (Y38 and S47) and missense mutation (R46). (a and b) Fab surface colored according to approximate net electrostatic potential (blue, positive; red, negative). Net positive charge seems to dominate, complementing the "acidic stretch" net negative charge (orange sphere: chloride ion). (c and d) Polar interactions in the sulfo-tyrosine specificity pocket. The sY38 of Pep4 (d) is directed into a small pocket formed by CDR-H3 where main chain H-atoms provide H-bonds to the sulfate group. The Y38 of Pep1 (c) adopts a slightly shifted side-chain position, the rest of the specificity pocket occupied by an apparent monoatomic entity with a number of electrons consistent with our assignment as chloride ion (orange sphere). A net positive partial charge supplied by the (unchanged) CDR-H3 main chain plus a halogen bond interaction with the Y38 hydroxyl seem to account for the presence of chloride. (e and f) Polar interactions at the peptides' C-terminal ends include a salt-bridge between R46 and heavy-chain E95. The phosphorylation of S47 leads to at least one additional H-bond with the Fab6E2 light chain, to N28 (f), in addition to the one with light-chain Y32 seen for Pep1 without modification of the serine (e). The relevance of interactions involving the Zn^{2+} ions (purple spheres) can be questioned since non-physiologically high concentrations were part of the crystallization medium.

variant R46L, resulted in complete loss of Ab6E2 binding (Table 1).

Pep6 contained the gain-of-function mutation E32K at its N-terminus. Its crystal structure revealed additional structured residues not observed in Pep1 and Pep4, where they were disordered. These are the three N-terminal amino acids (residues 32–34) including the missense mutation E32K, as well as and

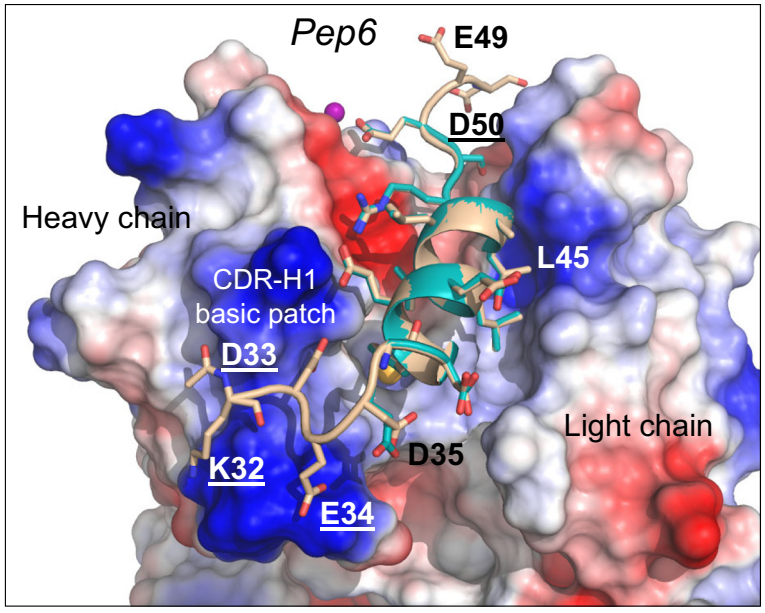

Fig. 4. Crystal structure of Pep6 (E32K mutation) in complex with Fab6E2. The Pep1 (wild-type, cyan) is superimposed on Pep6 (tan) of the Fab6E2:Pep6 complex with the Fab surface colored according to approximate net electrostatic potential (blue positive, red negative). The structured residues (K32–D33–E34 and D50) that were disordered in the Pep1 and Pep4 complexes are indicated and underlined. Purple sphere represents a Zn^{2+} ion, and the orange sphere represents a chloride ion.

the C-terminal residue D50 (Fig. 4), all of which are well resolved in the electron density map (1 sigma $2mF_o - F_c$). The N-terminal K32 and the C-terminal D50 are in contact with symmetry-related molecules in the crystal lattice, which may explain why they and the residues D33 and D34 are ordered in the structure. In addition, the aliphatic portion of the K32 side chain engages in van der Waals contacts to the Fab CDR-H1. The buried solvent-accessible surface of Pep6 is ~884 Å^2 and larger than that of Pep1 (~610 Å^2) and Pep4 (~680 Å^2), mainly due to the additional contributions from K32 (110 Å), D33 (66 Å^2), and E34 (67 Å^2) interactions with a basic patch formed by Fab6E2 CDR-H1 (Fig. 4). The structured region of Pep6 comprises the three residues subject to missense mutations (E32K, D35Y and R46L) and the two PTM sites, encompassing a length of 19 residues (K32–D50), which is about 2/3 of length of the entire acidic stretch (residues 31–60). Other than the extended length of the structured region, Pep6 is identical to the structures of Pep1 and Pep4, including the centrally positioned α-helix (Fig. 4).

The mouse PCSK9 sequence (^{40}DYEELMLAL PSQ^{51}) corresponding to the structured region of the human sequence (^{37}DYEELVLALRSE^{48}) has two important changes (murine M45 instead of human V42 and murine P49 instead of human R46), which likely preclude Ab6E2 binding. Indeed, SPR binding experiments showed that Ab6E2 bound neither to the mouse acidic stretch peptide Pep8 (Table 1) nor to the intact mouse PCSK9 (data not shown).

NMR studies indicate a propensity of the acidic stretch-derived peptide to adopt an α-helical conformation in solution

The chemical shift values of backbone atoms (Cα, C′, Hα) in proteins and peptides have been shown to correlate with the presence of elements of secondary structure. In particular, for Hα resonances, residues experiencing an upfield shift (i.e., smaller chemical shift value relative to the random coil value) are usually found in α-helical conformations, whereas a downfield shift (i.e., larger chemical shift value compared to the random coil value) is indicative of β-strand conformations [50].

The results with wild-type Pep1 showed that all of the amino acids in the region (^{39}EELVL^{43}) display chemical shift values smaller than the random coil values, indicating a propensity to adopt an α-helical conformation (Fig. 5a). It is important to point out that the extent of the observed deviations is smaller than what is typically observed for stable helical conformations (i.e., 0.15 to 0.6 ppm). This can be explained considering that the chemical shift values, like all NMR parameters, are population-weighted averages over all conformations in solution. Therefore, the smaller deviations observed for Pep1 reflect the average among all possible conformations including a small population in an α-helical conformation.

The nuclear Overhauser effect (NOE) is another NMR parameter that provides important structural information. Due to resonances overlap for Pep1, it was not possible to observe the complete pattern of

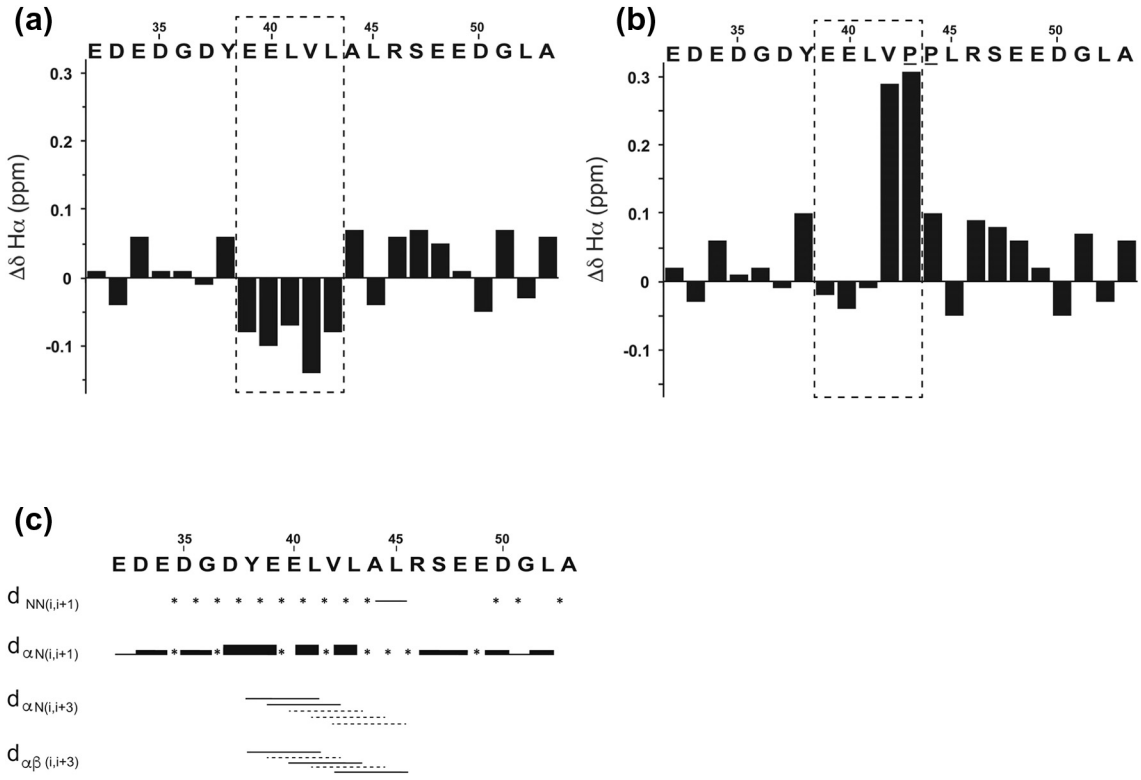

Fig. 5. NMR analysis of Pep1 (wild-type) and Pep10 (L43P:A44P) in solution. Differences between the Hα resonances (δ_{obs}) and the typical random coil values (δ_{rc}) for the corresponding amino acid type are reported as $\Delta\delta$ (= $\delta_{obs} - \delta_{rc}$) and are shown in panel a for Pep1 (wild-type) and in panel b for Pep10 (L43P:A44P). (c) Sequential and medium-range NOEs observed for Pep1 in PBS (pH 6.9) at 298 K. The thickness of the bars is proportional to the intensities of the NOE signals. Dashed lines and stars indicate correlations that could not be observed or unambiguously assigned due to resonance overlap.

NOEs characteristic of an α-helical structure. However, some weak medium-range NOE contacts, $d_{\alpha N\ (i,\ i+3)}$ and $d_{\alpha\beta(i,\ i+3)}$, were detected between a few amino acids spanning the region (^{38}YEELVLAL^{45}) (Fig. 5c), suggesting that only a small population of the peptide tends to adopt an α-helical conformation in this region of the sequence, consistent with the chemical shift results. Virtually identical results were obtained with peptides having the missense mutations D35Y (Pep9) and R46L (Pep7) (Suppl. Fig. S3). These two residues are situated beyond the limits of the helical segment, and as expected, the mutations did not affect the propensity to adopt a helical conformation.

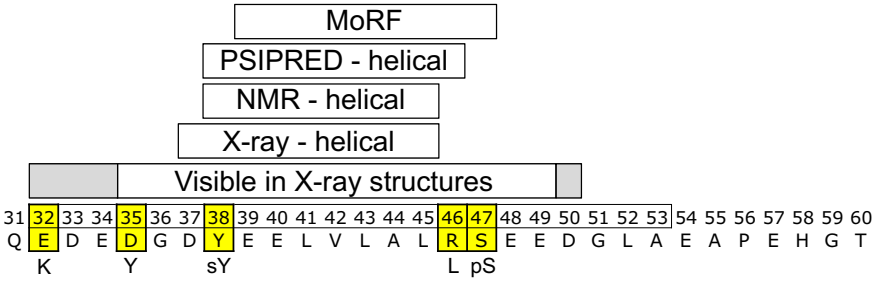

Fig. 6. Region of disorder-to-order transition in the acidic stretch of PCSK9. The IDR Q31–T60 contains gain- and loss-of-function mutations (E32K, D35Y, and R46L, respectively) and two PTM sites, sulfated Y38 (= sY) and phosphorylated S47 (= pS). The boxes indicate the structured and helical regions detected by X-ray and NMR, as well as the computationally predicted helix (PSIPRED) and the MoRF. The gray shaded boxes show structured segments only found in the crystal structure with Pep6 (E32K mutation). The peptides used for structural studies comprised residues 32–53 (boxed).

The region with α-helical propensity detected by NMR is a close match to the α-helical segment observed in the crystal structures (^{37}DYEELVLAL^{45}) (Fig. 6). In further agreement, the secondary structure prediction program PSIPRED (http://bioinf.cs.ucl.ac.uk/psipred/) [51,52] assigns a helical region within the acidic stretch that corresponds to our experimentally determined α-helical sequence (Fig. 6). Therefore, the herein identified structured segment within the disordered acidic stretch conforms to the proposed concept of MoRFs, which are short segments within a disordered region that undergo structural folding to interact with a binding partner [21,27,53]. Indeed, MoRFpred (http://biomine.cs.vcu.edu/servers/MoRFpred/), a computational MoRF prediction tool [53], identified the acidic stretch segment E39-S47 as a MoRF (Fig. 6), closely matching the structured region identified by NMR and crystallography.

Evidence that the acidic stretch of the PCSK9 protein can adopt an α-helical conformation

It was important to experimentally demonstrate that the α-helical conformation is not limited to peptides, but that it also occurs in PCSK9 protein. We considered that Ab6E2 may specifically recognize the helical conformation rather than an extended non-helical conformation of the acidic stretch region. The crystal structures predict that an extended conformation of the peptides would be unable to bind to Ab6E2, due to the loss of the helix-dependent positioning of the key contact residues. Therefore, the disruption of the helix by introduction of helix-breaking proline residues should result in a loss of binding. Guided by

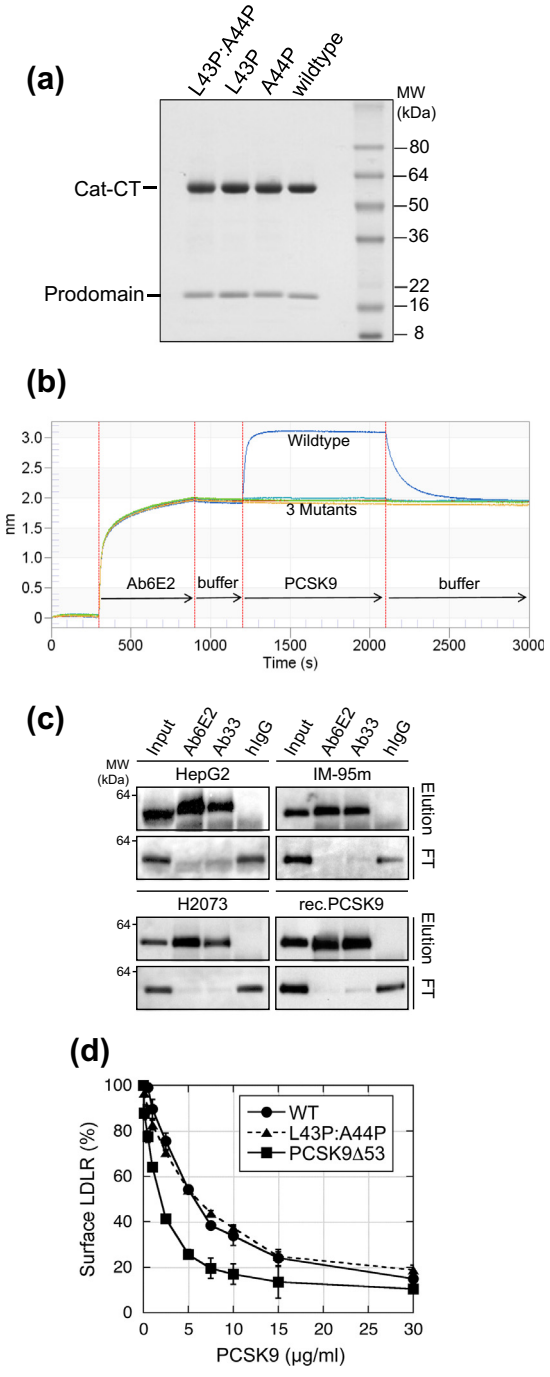

Fig. 7. The acidic stretch α-helix, detected by Ab6E2, is formed in native PCSK9 protein but is not required for auto-inhibitory activity. (a) SDS-PAGE (non-reducing conditions) and Coomassie® staining of CHO-expressed and purified proline mutants and wild-type PCSK9, all having an intact prodomain (Cat-CT = catalytic/C-terminal domain of PCSK9). (b) Biolayer interferometry of Ab6E2 binding to wild-type PCSK9 and proline mutants. Ab6E2 was immobilized on an anti-hIgG Fc sensor on an Octet Red384 biolayer interferometry system and washed in buffer to establish a baseline before adding the PCSK9 proteins. Binding kinetics show that none of the three mutants (PCSK9–L43P, PCSK9–A44P, PCSK9–L43P:A44P) had any detectable binding at a concentration of 250 nM, which gave saturation binding to wild-type PCSK9. (c) Immunoprecipitation of secreted native PCSK9 from HepG2, IM-95m, and H2073 cell lines and of rec.PCSK9 using Ab6E2 and the control antibody Ab33, which recognizes the EGF(A)-binding region of PCSK9. Antibodies were immobilized on magnetic beads and incubated with concentrated cell culture media, and bound PCSK9 was eluted. Recovered PCSK9 in the elution fraction (Elution) and in the flow-through (FT) was detected with the polyclonal anti-Cat Ab (as in Fig. 1a), showing that native PCSK9 was efficiently bound by both antibodies. Rec.PCSK9 and human IgG (hIgG) were used as experimental controls. Results are representative of three independent experiments. (d) PCSK9-mediated degradation of surface LDLR on HepG2 cells. HepG2 cells were incubated for 4 h with increasing concentrations of wild-type PCSK9 (WT), the double proline mutant PCSK9–L43P:A44P, and the acidic stretch deletion mutant PCSK9Δ53 and LDLR surface levels were determined by FACS using anti-LDLR antibody. The results are the average of three independent experiments ± SD.

the structures, we chose L43 and A44 for mutagenesis experiments because these residues are surface-exposed and not involved in direct Ab6E2 interactions. To ascertain that the introduced proline changes indeed abolished the helical conformation, we examined Pep10 (L43P:A44P) by solution NMR. The mutations caused major chemical shifts approaching values of random coil in the region 39–43, which is the core of the α-helical region in the wild-type peptide, whereas little or no effects were observed for residues 32–37 and 45–53 located outside this region (Fig. 5b). Moreover, no medium-range NOEs characteristic of an α-helix were observed, indicating that the introduction of two proline residues in Pep10 obliterated any propensity to form an α-helical structure. SPR binding experiments clearly demonstrated that this peptide, as well as peptides with individual proline mutations, Pep11 (L43P) and Pep12 (A44P), had no detectable binding to Ab6E2 (Table 1).

The corresponding proline mutants were then introduced into the PCSK9 protein (PCSK9–L43P, PCSK9–A44P, and PCSK9–L43P:A44P), which were expressed in CHO cells and purified. The prodomain was not degraded during the purification process but remained fully intact in all mutants (Fig. 7a). Biolayer interferometry experiments demonstrated that at a concentration of 250 nM, at which the binding of wild-type PCSK9 to Ab6E2 was saturated, the PCSK9 mutants did not produce any detectable binding signal (Fig. 7b), indicating that the formation of a proper α-helix is required for the binding interaction. Therefore, the specific recognition of the helical conformation makes Ab6E2 an excellent probe to investigate the prevalence of this acidic stretch helix in native PCSK9 forms. For this, we performed pull-down experiments using conditioned media from HepG2, IM-95m, and H2073 cells as well as rec.PCSK9 expressed in CHO cells. Figure 7c shows that Ab6E2 and the positive control antibody Ab33, which binds to the EGF(A)-binding region of the catalytic domain [54], were able to pull down native PCSK9 as well as rec.PCSK9 in a quantitative fashion. The Ab6E2 was able to capture the majority of the PCSK9 protein, as indicated by the depletion of PCSK9 in the flow-through samples. The results suggested that the formation of the helical conformation is a general property of PCSK9, independent of its cellular origin.

Moreover, if the α-helical conformation is important for the auto-inhibitory function of the acidic stretch, then the helix-abolishing proline mutations should lead to increased LDLR degradation in HepG2 cells. PCSK9Δ53, which represents the hyperactive PCSK9 form, was significantly more potent in down-regulating surface LDLR levels compared to the wild-type PCSK9 (Fig. 7d), consistent with published data [37,46]. However, the double proline mutant PCSK9–L43P:A44P did not show improved potency (Fig. 7d), suggesting that the α-helix is not critical for this particular function.

Discussion

The interest in the PCSK9 acidic stretch, which so far has eluded structural characterization, is heightened by the presence of missense mutations and PTM sites. The herein presented findings demonstrate that a segment within the unstructured acidic stretch is able to undergo disorder-to-order transition, which is consistent with computational secondary structure predictions. Structural studies with acidic stretch-derived peptides demonstrated that the Y38–L45 segment had the propensity to adopt an α-helix, which is further stabilized upon binding to the ligand Fab6E2. The observed helical structure is not limited to peptides, but is a true property of the acidic stretch in the PCSK9 protein, as indicated by studies with helix-breaking PCSK9 mutants. An immediate consequence of helix formation is that the linear sequence containing the missense mutations and PTM sites becomes ordered and compressed. In addition, the helical structure spatially orients the missense mutations and PTM residues, which seem primed to interact with a protein ligand(s) in a conformation-specific manner.

According to the classification system of IDRs, the PCSK9 acidic stretch is an α-MoRF, which is a short interaction-prone segment within a disordered region that adopts a helical conformation upon interaction with a binding partner [20,55]. In agreement with the general features of α-MoRFs exemplified by the family of BH3-only proteins [29], the helical segment within the acidic stretch is enriched in hydrophobic residues, which form the Fab6E2 binding interface. Furthermore, akin to the PCSK9 acidic stretch, the N-terminal region of the transcriptional activator C/EBP-homologous protein (CHOP) is disordered and highly acidic with a 20% content of glutamic acid residues [56]. NMR studies showed that this region also undergoes ordering of two segments that have α-helical propensity and are enriched in hydrophobic residues believed to be critical for macromolecular recognition during transcriptional activation [56]. Thus, it is possible that the structure-prone region of the PCSK9 acidic stretch including the α-helix may also interact with a physiological binding partner. In this respect, the surrogate binding partner Ab6E2 may mimic some aspects of a physiological ligand, since the sulfation of the Y38 residue affords a remarkably strong binding affinity to Fab6E2 (K_D 1.9 nM). Tyrosine sulfation is a known modifier of protein–protein interactions as exemplified by the chemokine receptor family [57]. For instance, the N-terminus of the well-studied chemokine receptor CCR5 harbors several tyrosine sulfation sites, which are critical for

the high-affinity binding to chemokine ligands and to the CD4/gp140 complex [57–60]. Akin to the PCSK9 acidic stretch, the tyrosine-sulfated N-terminal segment of CCR5 is disordered with a propensity to form an α-helix, which is stabilized upon binding to the protein partner [60,61]. In analogy, it is conceivable that the PCSK9 α-helix presents the sY38 residue to engage in interactions with a physiological ligand.

The transition of the PCSK9 acidic stretch segment Y38–L45 into an α-helix is not required for the auto-inhibitory function, since the helix-breaking PCSK9 mutant (L43P:A44P) maintained auto-inhibitory activity in a cellular assay. Our conclusion that helix formation is dispensable for auto-inhibition is in agreement with a previous study showing that the excision of the segment L41-L45, which is part of the helical segment, did not affect the auto-inhibitory activity [46]. This suggests that the helical state may be relevant for functions other than auto-inhibition, perhaps related to the biology of the missense mutations and the PTMs. Therefore, the acidic stretch may have different functions that are associated with the disordered and the ordered states. Auto-inhibition does not require any specific structural and sequence features [37,46] since the entire acidic stretch could be functionally replaced by an unrelated disordered segment of similar length and negative charge [37]. This strongly suggests that auto-inhibition is mediated by the disordered state of the negatively charged acidic stretch. The extended conformation of the acidic stretch (~114 Å) would be able to reach functionally important sites on PCSK9 *in-cis* and interfere with PCSK9 activity to explain its auto-inhibitory function in LDLR binding assays and in cellular LDLR degradation assays [8,37,46]. These are the prodomain contact site with the LDLR-β-propeller domain, the C-terminal domain of PCSK9, and the EGF(A) binding site on the PCSK9 catalytic domain (Fig. S1A). However, the most attractive site within binding distance of the disordered acidic stretch is a positively charged patch on the prodomain [10] (Fig. S1A). Its interaction with negatively charged heparan sulfate proteoglycans on the cell surface enhances PCSK9 binding to LDLR and LDLR degradation [10]. Therefore, occupancy of this basic interaction patch by the acidic stretch would afford auto-inhibition by preventing the binding of PCSK9 to the cell surface heparan sulfate proteoglycans. However, this hypothesis is tempered by the findings by Ly *et al*. [11], showing that the cell surface proteoglycan glypican-3 is a negative rather than a positive regulator of PCSK9 binding to LDLR.

On the other hand, the ordering of the acidic stretch segment comprising a central α-helix may provide specific molecular interactions with putative binding partner(s), extracellular or intracellular, and the missense mutations or PTMs may either facilitate or impair such interaction to modify PCSK9 function. It is conceivable that this ordered state could play a role in the interaction of PCSK9 with LDL particles, since this interaction depends on the presence of the acidic stretch region [45]. The exact nature of the binding partner on LDL particles has not been elucidated, but it was suggested that either the major structural protein ApoB100 or another protein carried by LDL particles, rather than lipids, may constitute the PCSK9 ligand [45]. It remains to be seen whether this interaction is dependent on the helical conformation of the acidic stretch and how missense mutations or PTMs would influence the binding.

The herein reported identification of a helix-prone segment within the acidic stretch and its binding to a surrogate Fab ligand does not prove the existence of specific physiological binding partner(s). However, it presents an intriguing framework for future studies aiming to elucidate the molecular mechanisms associated with the function of missense mutations and PTMs located in the acidic stretch region.

Materials and Methods

Structure determination of Fab6E2–peptide complexes

The chimeric Fab6E2 was expressed in *Escherichia coli*, and frozen cell paste was thawed in lysis buffer containing PBS/2.5 mM EDTA and 1 mM PMSF. Cells were homogenized with the use of a Tissuemizer (30 s), and the resulting slurry was passed through a microfluidizer (Microfluidics) twice. Insoluble matter was pelleted by centrifugation. Clarified lysate was loaded onto a Protein G column (catalog no. 17-0618-05; GE Healthcare) at 5 ml/min. The column was then washed with lysis buffer before eluting Fab6E2 with elution buffer (0.58% acetic acid). Eluted Fab6E2 fractions were loaded onto a 5-ml prepacked SPHP column (GE Healthcare, catalog no. 17-1152-01), which had been pre-equilibrated with buffer A [20 mM Mes (pH 5.5)]. After washing with buffer A, bound Fab6E2 was eluted with buffer B [20 mM Mes (pH 5.5), 0.5 M NaCl] using a gradient from 0% to 100% buffer B in 20 column volumes. The fractions containing Fab6E2 were analyzed by SDS-PAGE, pooled and desalted using PD10 G25 M Tris-buffered saline, and then concentrated to 10 mg/ml. The complexes of Fab6E2 with unmodified Pep1 (wild-type) with modified Pep4 (sY38, pS47) and Pep6 (E32K) were formed by combining Fab and peptide in a 2-fold molar excess of peptide and incubation on ice for 1 h. After screening for crystallization conditions by vapor diffusion using commercially available kits in sitting drops, optimized crystals were grown in hanging drops. The unmodified and modified peptide complex crystals arose from a 1:1 mixture of protein/peptide stock with 15% PEG8K, 0.2 M zinc acetate,

and 0.1 M sodium cacodylate (pH 6.5). After immersion in reservoir made 35% in meso-erythritol, a crystal was preserved for data collection by sudden immersion into liquid nitrogen.

Diffraction data for the Pep1 complex extending to 2.25 Å were collected at ALS beamline 5.0.2 and processed using HKL2000 [62] in an orthorhombic lattice. The structure of a one-complex asymmetric unit was solved using molecular replacement in two steps. A series of rotation function calculations applied a set of Fabs in which the elbow angle was crudely incremented in 5° steps across 100°. A well-discriminated model having been identified by a maximum RFZ value, an automatic homology-building pipeline using Modeller [63], and PDB entry 1QYG was used to provide a sequence-corrected version of the preferred Fab. This model served as search probe for a full molecular replacement search after deletion of CDR residues, a clear solution resulting in space group $P2_12_12$. Some limited model building (Coot [64]) and refinement (Refmac5 [65]) provide electron density maps with strong indications of the PCSK9 peptide. Prominent positive features in $mF_o - F_c$ maps were fitted as zinc ions or in one case as chloride ion. The chloride ion position was also tested as a water and as a sulfate ion. In these tests, $mF_o - F_c$ map features indicated water assigned too few elections and the sulfate ion too many electrons. A prominent appendage to the side chain of heavy-chain H58 (Kabat numbering) led to the assignment of this amino acid as phospho-histidine. Mass spectrometric analysis of the purified Fab6E2 was consistent with an unmodified H58. Thus, we suspect that phospho-H58 was formed in the crystallization medium (samples from crystals were not successfully ionized in mass analysis experiments). A residual $mF_o - F_c$ feature adjacent to the light-chain N-terminal aspartic acid bears more electrons than an alanine residue (based on test refinement and map inspection) and may also reflect a phosphorylation event, but such a feature is not included in the structure. Final refinements employed BUSTER [66] and phenix.refine [67].

Diffraction data for the Pep4 complex with Fab6E2 extending to 2.20 Å were collected at APS beamline 22-ID using 1.0000 Å X-rays and reduced in a lattice isomorphous with that from the Pep1 complex. The structure of Fab6E2 with Pep4 was solved by molecular replacement using the previously determined Fab6E2 structure, without peptide. The initial electron density maps provided strong evidence for a peptide with extra density for Y38 and S47 side chains. Simulated annealing refinement and model building and refinement led to the incorporation of zinc ions, sulfo-tyrosine at peptide residue 38, a (two-fold) disordered phospho-serine for peptide residue 47, and a disorder model for heavy-chain residue H58 that included phosphorylation at each of the side-chain nitrogen atoms. Simulated annealing omit maps were applied to the study of the phospho-serine and phospho-histidine residues but without leading to an improved model. Some zinc ion positions were tested with cacodylate ions, but the final model considers these sites to be zinc ions. Final refinements employed phenix.refine [67]. Metrics from data reduction and refinement are in Suppl. Table S1.

The most significant features in a difference electron density map with coefficients mF_o(modified) – F_o (unmodified) phased using the unmodified Pep1 structure were as follows: SO_3 group on Y38, combination of sulfate and zinc ions near light-chain residues N155 and H189, a Zn^{2+} near pS47, a negative feature near the light-chain N-terminal D1, the PO_3 of pS47, a collection of features consistent with a shift of CDR-L3 away from CDR-H2, and a collection of features consistent with a shift of CDR-L1 away from the modified version of the peptide.

Diffraction data for the Pep6 complex with Fab6E2 extending to 2.10 Å were collected at APS beamline 24-IDC using 1.0000 Å X-rays and reduced in a lattice isomorphous with the Pep1 complex. The structure of Fab6E2 with Pep6 was solved by molecular replacement using the previously determined Fab6E2 structure, without peptide. The initial electron density maps provided strong evidence for a peptide with extra density for K32, D33, and E34 side chains. Simulated annealing refinement and model building and refinement led to the incorporation of zinc ions and one chloride ion and a disorder model for heavy-chain residue H58 that included phosphorylation at each of the side-chain nitrogen atoms. Simulated annealing omit maps were applied to the study the addition of the N-terminal acetyl group as well as two C-terminal residues Glu49 and Asp50 to an improved model. Final refinements employed BUSTER [66] and phenix.refine [67] Metrics from data reduction and refinement are in Suppl. Table S1.

Proteins, antibodies, and peptides

The human PCSK9 mutants PCSK9–L43P, PCSK9–A44P, and PCSK9–L43P:A44P and the deletion mutant PCSK9Δ53 (deletion of Q31–A53) were constructed based on wild-type PCSK9 having a C-terminal His8-tag [54], using site-directed mutagenesis. DNA encoding for mouse PCSK9 (M1-Q694) with C-terminal His8-tag and with EcoRI (5′) and XbaI (3′) endonuclease cleavage sites was generated by PCR using mouse PCSK9 cDNA (GenBank BC038085) as a template. The PCR fragment encoding mouse PCSK9 was treated with endonuclease EcoRI and XbaI and inserted into a mammalian expression vector (pRK5) with a cytomegalovirus promoter using standard molecular biology techniques. The sequence was verified by DNA sequencing. The wild-type human PCSK9 [54] (= PCSK9),

PCSK9 mutants and mouse PCSK9 were expressed by transient transfection of Chinese hamster ovary (CHO) cells and purified from conditioned media by affinity chromatography using a nickel–nitrilotriacetic acid–agarose column (Qiagen) followed by gel filtration on a Sephacryl S-200 column (GE Healthcare) as described [54]. Peptides were synthesized by CPC Scientific or by the peptide synthesis group at Genentech, and all N–termini were acetylated and all C–termini were amidated.

Anti-PCSK9 antibody Ab6E2 was identified by immunizing PCSK9$^{-/-}$ mice with recombinant human PCSK9 as described for the antibodies 3D5 and 7G7 [48]. Total RNA was extracted from hybridoma cells producing Ab6E2 mouse monoclonal antibody (RNeasy Mini Kit; Qiagen). Using SMARTer RACE cDNA Amplification Kit (Clontech), the RNA was first reverse transcribed, followed by first-strand cDNA synthesis and 5′ RACE PCR amplification of the variable light (VL) and variable heavy (VH) domains with gene-specific primers. The identified VL and VH domains were inserted into a pBR322-derived *E. coli* expression vector with human kappa CL and CH1 domains. This chimeric Fab6E2 was expressed in *E. coli* using shake flask cultures. The expression plasmid was transformed into 64B4 *E. coli* expression strain, and colonies were inoculated into Luria–Bertani supplemented with 50 μg/ml carbenicillin and grown at 30 °C with shaking for 16 h. The culture was then diluted 100-fold into 50 ml of complete C.R.A.P. medium supplemented with 50 μg/ml carbenicillin in a baffled, vented flask. The culture was grown at 30 °C with shaking at 200 rpm for 24 h, after which the cell pellet was collected and frozen for subsequent Fab6E2 purification (see above under "Structure determination of Fab6E2–peptide complexes"). To generate chimeric mouse/human IgG1, the VL and VH domains were subcloned into pRK mammalian expression vectors encoding the human kappa and γ1 constant domain, respectively [68]. This chimeric full-length antibody, designated as Ab6E2, was transiently expressed in CHO cells and purified on a protein A column.

NMR spectroscopy

NMR experiments were carried out on a Bruker DRX-600 equipped with a triple-resonance cryoprobe. Samples for NMR studies were prepared by dissolving the PCSK9 peptides (Pep1, Pep7, Pep9, and Pep10) in PBS (10% D_2O or 100% D_2O) at pH 6.9 to a final concentration of 0.8–1.5 mM. All NMR spectra were collected at 298 K and internally referenced to DSS (4,4-dimethyl-4-silapentane-1-sulfonic acid). Complete assignment of the proton resonances was achieved using a combination of 2D TOCSY, 2D DQFCOSY, and 2D NOESY experiments. The mixing times for the TOCSY and NOESY spectra were 90 and 200 ms, respectively. The NMR data were processed using the NMRPipe/NMRDraw package [69] and analyzed with NMRView [70].

Cell surface LDLR assay with HepG2 cells

The potencies of PCSK9, PCSK9Δ53, and PCSK9–L43P:A44P on LDLR degradation in HepG2 cells were measured as described [48] by using serially diluted PCSK9 proteins and a 4-h incubation period. The results presented are the average ± SD of three independently performed experiments.

SPR for Ab6E2 binding to PCSK9, PCSK9Δ53, and mouse PCSK9

Ab6E2 was immobilized on a protein A sensor chip (GE Healthcare), and binding kinetics of PCSK9, PCSK9Δ53, and mouse PCSK9 (1–250 nM) in HBS-EP buffer (GE Healthcare) were measured on a Biacore S200 instrument. The data were well described by a 1:1 binding model. The determined kinetic constants were the averages of three independent experiments. The K_D values, calculated from the determined k_{on} and k_{off} values, were the average ± SD of three independent experiments.

SPR for peptide binding to Ab6E2

Affinity constants were measured using a Biacore T100 at 20 °C. Briefly, recombinant protein A/G (Thermo Scientific, no. 21186) was amine-coupled onto a CM5 sensor chip according to manufacturer's instructions to a density of approximately 3000 RU. The assay buffer contained 50 mM Hepes, 150 mM NaCl, 0.005% Tween 20, 0.1 mg/ml ovalbumin, and 4.0% DMSO (pH 7.2). Ab6E2 (100 nM) was injected over channel 2 to a capacity of >3000 RU, and channel 1 remained uncoated with target in order to provide a reference response. Five serial dilutions in triplicate of each peptide were prepared in assay buffer starting at 20 μM, except for Pep2 and Pep4, which were prepared from a 100-nM starting solution. Peptides were injected at a rate of 50 μl/min for 30 s (or 100 s for Pep2 and Pep4) from low-to-high concentration using a five-step single cycle kinetics format. After a variable dissociation period (i.e., 2 min for weak binders and 10 min for strong binders), bound Ab6E2–peptide complexes were removed by injecting 10 mM glycine at pH 1.5 for 30 s. This sequence of seven injections was composed of a single cycle that was repeated for each peptide as duplicates, which were essentially superimposable and were fit to a simple 1:1 binding interaction model to obtain a single affinity value for each peptide, as presented in Table 1. Affinity for Pep2 was similarly determined but from a separate assay run employing the same methodology because of interference from air spikes. Blank curve sets were obtained by running samples that did not contain peptide using

the same procedure. The data were double referenced, and duplicate curves were globally fitted with a 1:1 binding interaction model using Biaevaluation version 2.0.4.

Biolayer interferometry for binding of PCSK9 proline mutants to Ab6E2

All experiments were carried out on an Octet Red384 system (Pall ForteBio). Ab6E2 was immobilized on an anti-hIgG Fc sensor (Pall ForteBio), and association and dissociation kinetics were measured for PCSK9, PCSK9–L43A, PCSK9–A44A, and PCSK9–L43P:A44P (all at 250 nM) in 50 mM Tris (pH 7.5), 300 mM NaCl, 2 mM $CaCl_2$, 1 mg/ml BSA, and 0.1% Tween-20. Kinetic data curves were generated by Octet software Version 9.0 (Pall ForteBio).

Protein immunoblotting

Secreted PCSK9 in conditioned media was detected by use of direct immunoblotting and compared with rec.PCSK9 and PCSK9Δ53. Media and proteins were diluted in PBS, resolved by SDS-PAGE using Novex Wedge Well 4%–20% Tris–glycine gel, and transferred to nitrocellulose membranes by dry transfer (iBind; Thermo Fisher Scientific) according to the manufacturer's protocol. PCSK9 was detected using the following antibodies: Ab6E2 followed by secondary antibody goat anti-human–IgG HRP (Thermo Fisher Scientific) and anti-Cat antibody (a rabbit polyclonal antibody that recognizes the N-terminal region, i.e., the P′-helix, of the PCSK9 catalytic domain [54]) followed by secondary antibody anti-rabbit IgG HRP (GE Healthcare). Secondary antibodies were detected using enhanced chemiluminescence (ECL Plus; General Electric Healthcare).

Cell culture

The HepG2, NCI-H2073, and the IM-95m cell lines were purchased from American Type Culture Collection (Manassas, VA) and the JCRB Cell Bank (Osaka, Japan), respectively. The cells were cultured in 50:50 F-12/DMEM media (Corning) supplemented with 10% ultra-low IgG FCS (Gibco) and 10 mM Hepes (pH 7.4) in T175 tissue culture flasks (Thermo Fisher Scientific). All cell lines were cultured at 37 °C in 5% CO_2 humidity to >80% confluence. Cells were washed three times with 20 ml PBS, and the media was replaced with 50:50 F-12/DMEM and 10 mM Hepes (pH 7.4). Conditioned media containing secreted PCSK9 was collected after 3 days of culture and concentrated 100-fold using Amicon Ultra-15 (Millipore Sigma, Darmstadt) with a 30-kDa cutoff.

Immunoprecipitation

Immunoprecipitation was performed using antibodies Ab6E2, Ab33 (a monoclonal antibody that binds to the PCSK9 catalytic domain [54]; positive control), and hIgG (negative control; anti-HGFA Ab75 [71]) immobilized onto magnetic Protein G Dynabeads (Thermo Fisher Scientific) according to the manufacturer's protocol. Concentrated media and rec.PCSK9 were diluted in PBS containing 0.1% Tween-20 (PBST). A portion of the diluted samples was taken ("input"), and the remainder was incubated with immobilized antibodies for 30 min at 4 °C. The flow through was collected, and the beads were washed three times with PBST. Captured PCSK9 was eluted by incubation in PBST containing 0.1% SDS and 50 μM TCEP for 10 min at 95 °C. The input, flow through, and eluate were analyzed on Novex Wedge Well 10%–20% Tris–glycine gel (Thermo Fisher Scientific) and transferred to nitrocellulose membranes, and PCSK9 was detected using anti-Cat antibody followed by anti-rabbit IgG HRP (GE Healthcare). Secondary antibodies were detected as described above.

Acknowledgments

We thank Tao Sai and Joyce Lai for the hybridoma work on the 6E2 antibody. Synchrotrons at the ALS and the APS are supported by the Director, Office of Science, Office of Basic Energy Sciences, of the U.S. Department of Energy (DOE) under contracts DE-AC02-05CH11231 and DE-AC02-06CH11357, respectively. The Berkeley Center for Structural Biology is supported in part by the NIH, NIGMS, and the HHMI. Supporting institutions of the Southeast Regional Collaborative Access Team 22-ID may be found at www.ser-cat.org/members.html. For NE-CAT 24-IDC, the work was based upon research conducted at the Northeastern Collaborative Access Team beamlines, which are funded by the National Institute of General Medical Sciences from the National Institutes of Health (P30 GM124165). The Pilatus 6M detector on 24-ID-C beam line is funded by a NIH-ORIP HEI grant (S10 RR029205). This research used resources of the Advanced Photon Source, a US DOE Office of Science User Facility operated for the DOE Office of Science by Argonne National Laboratory under Contract No. DE-AC02-06CH11357.

Appendix A. Supplementary data

Supplementary data to this article can be found online at https://doi.org/10.1016/j.jmb.2018.11.025.

Received 16 July 2018;
Received in revised form 6 November 2018;
Accepted 26 November 2018
Available online 15 January 2019

Keywords:
proprotein convertase;
LDL receptor;
posttranslational modifications;
intrinsically disordered regions;
molecular recognition motif

Abbreviations used:
PCSK9, proprotein convertase subtilisin/kexin 9; LDLR, LDL receptor; EGF(A), epidermal growth factor-homology domain-A; PTM, posttranslational modification; SPR, surface plasmon resonance; CDR, complementarity determining region; NOE, nuclear Overhauser effect; IDR, intrinsically disordered region; MoRF, molecular recognition feature.

References

[1] N.G. Seidah, Z. Awan, M. Chretien, M. Mbikay, PCSK9: a key modulator of cardiovascular health, Circ. Res. 114 (2014) 1022–1036.
[2] N.G. Seidah, S. Benjannet, L. Wickham, J. Marcinkiewicz, S.B. Jasmin, S. Stifani, A. Basak, A. Prat, M. Chretien, The secretory proprotein convertase neural apoptosis-regulated convertase 1 (NARC-1): liver regeneration and neuronal differentiation, Proc. Natl. Acad. Sci. U. S. A. 100 (2003) 928–933.
[3] M. Abifadel, M. Varret, J.P. Rabes, D. Allard, K. Ouguerram, M. Devillers, C. Cruaud, S. Benjannet, L. Wickham, D. Erlich, A. Derre, L. Villeger, M. Farnier, I. Beucler, E. Bruckert, J. Chambaz, B. Chanu, J.M. Lecerf, G. Luc, P. Moulin, J. Weissenbach, A. Prat, M. Krempf, C. Junien, N.G. Seidah, C. Boileau, Mutations in PCSK9 cause autosomal dominant hypercholesterolemia, Nat. Genet. 34 (2003) 154–156.
[4] J. Cohen, A. Pertsemlidis, I.K. Kotowski, R. Graham, C.K. Garcia, H.H. Hobbs, Low LDL cholesterol in individuals of African descent resulting from frequent nonsense mutations in PCSK9, Nat. Genet. 37 (2005) 161–165.
[5] J.C. Cohen, E. Boerwinkle, T.H. Mosley Jr., H.H. Hobbs, Sequence variations in PCSK9, low LDL, and protection against coronary heart disease, N. Engl. J. Med. 354 (2006) 1264–1272.
[6] I.K. Kotowski, A. Pertsemlidis, A. Luke, R.S. Cooper, G.L. Vega, J.C. Cohen, H.H. Hobbs, A spectrum of PCSK9 alleles contributes to plasma levels of low-density lipoprotein cholesterol, Am. J. Hum. Genet. 78 (2006) 410–422.
[7] D.W. Zhang, T.A. Lagace, R. Garuti, Z. Zhao, M. McDonald, J.D. Horton, J.C. Cohen, H.H. Hobbs, Binding of proprotein convertase subtilisin/kexin type 9 to epidermal growth factor-like repeat A of low density lipoprotein receptor decreases receptor recycling and increases degradation, J. Biol. Chem. 282 (2007) 18602–18612.
[8] H.J. Kwon, T.A. Lagace, M.C. McNutt, J.D. Horton, J. Deisenhofer, Molecular basis for LDL receptor recognition by PCSK9, Proc. Natl. Acad. Sci. U. S. A. 105 (2008) 1820–1825.
[9] P. Lo Surdo, M.J. Bottomley, A. Calzetta, E.C. Settembre, A. Cirillo, S. Pandit, Y.G. Ni, B. Hubbard, A. Sitlani, A. Carfi, Mechanistic implications for LDL receptor degradation from the PCSK9/LDLR structure at neutral pH, EMBO Rep. 12 (2011) 1300–1305.
[10] C. Gustafsen, D. Olsen, J. Vilstrup, S. Lund, A. Reinhardt, N. Wellner, T. Larsen, C.B.F. Andersen, K. Weyer, J.P. Li, P.H. Seeberger, S. Thirup, P. Madsen, S. Glerup, Heparan sulfate proteoglycans present PCSK9 to the LDL receptor, Nat. Commun. 8 (2017) 503.
[11] K. Ly, R. Essalmani, R. Desjardins, N.G. Seidah, R. Day, An unbiased mass spectrometry approach identifiesgGlypican-3 as an interactor of proprotein convertase subtilisin/kexin type 9 (PCSK9) and low density lipoprotein receptor (LDLR) in hepatocellular carcinoma cells, J. Biol. Chem. 291 (2016) 24676–24687.
[12] G. Mayer, S. Poirier, N.G. Seidah, Annexin A2 is a C-terminal PCSK9-binding protein that regulates endogenous low density lipoprotein receptor levels, J. Biol. Chem. 283 (2008) 31791–31801.
[13] N.G. Seidah, S. Poirier, M. Denis, R. Parker, B. Miao, C. Mapelli, A. Prat, H. Wassef, J. Davignon, K.A. Hajjar, G. Mayer, Annexin A2 is a natural extrahepatic inhibitor of the PCSK9-induced LDL receptor degradation, PLoS One 7 (2012), e41865. .
[14] D.W. Zhang, R. Garuti, W.J. Tang, J.C. Cohen, H.H. Hobbs, Structural requirements for PCSK9-mediated degradation of the low-density lipoprotein receptor, Proc. Natl. Acad. Sci. U. S. A. 105 (2008) 13045–13050.
[15] O.L. Holla, J. Cameron, K. Tveten, T.B. Strom, K.E. Berge, J.K. Laerdahl, T.P. Leren, Role of the C-terminal domain of PCSK9 in degradation of the LDL receptors, J. Lipid Res. 52 (2011) 1787–1794.
[16] Y.G. Ni, J.H. Condra, L. Orsatti, X. Shen, S. Di Marco, S. Pandit, M.J. Bottomley, L. Ruggeri, R.T. Cummings, R.M. Cubbon, J.C. Santoro, A. Ehrhardt, D. Lewis, T.S. Fisher, S. Ha, L. Njimoluh, D.D. Wood, H.A. Hammond, D. Wisniewski, C. Volpari, A. Noto, P. Lo Surdo, B. Hubbard, A. Carfi, A. Sitlani, A proprotein convertase subtilisin-like/kexin type 9 (PCSK9) C-terminal domain antibody antigen-binding fragment inhibits PCSK9 internalization and restores low density lipoprotein uptake, J. Biol. Chem. 285 (2010) 12882–12891.
[17] E. Weider, D. Susan-Resiga, R. Essalmani, J. Hamelin, M.C. Asselin, S. Nimesh, Y. Ashraf, K.L. Wycoff, J. Zhang, A. Prat, N.G. Seidah, Proprotein convertase subtilisin/kexin type 9 (PCSK9) single domain antibodies are potent inhibitors of low density lipoprotein receptor degradation, J. Biol. Chem. 291 (2016) 16659–16671.
[18] D. Cunningham, D.E. Danley, K.F. Geoghegan, M.C. Griffor, J.L. Hawkins, T.A. Subashi, A.H. Varghese, M.J. Ammirati, J. S. Culp, L.R. Hoth, M.N. Mansour, K.M. McGrath, A.P. Seddon, S. Shenolikar, K.J. Stutzman-Engwall, L.C. Warren, D. Xia, X. Qiu, Structural and biophysical studies of PCSK9 and its mutants linked to familial hypercholesterolemia, Nat. Struct. Mol. Biol. 14 (2007) 413–419.
[19] M.S. Sabatine, R.P. Giugliano, A.C. Keech, N. Honarpour, S. D. Wiviott, S.A. Murphy, J.F. Kuder, H. Wang, T. Liu, S.M. Wasserman, P.S. Sever, T.R. Pedersen, Committee, F. S. & Investigators, Evolocumab and clinical outcomes in patients with cardiovascular disease, N. Engl. J. Med. 376 (2017) 1713–1722.
[20] A.K. Dunker, C.J. Oldfield, J. Meng, P. Romero, J.Y. Yang, J.W. Chen, V. Vacic, Z. Obradovic, V.N. Uversky, The

unfoldomics decade: an update on intrinsically disordered proteins, BMC Genomics 9 (Suppl. 2) (2008) S1.
[21] R. van der Lee, M. Buljan, B. Lang, R.J. Weatheritt, G.W. Daughdrill, A.K. Dunker, M. Fuxreiter, J. Gough, J. Gsponer, D.T. Jones, P.M. Kim, R.W. Kriwacki, C.J. Oldfield, R.V. Pappu, P. Tompa, V.N. Uversky, P.E. Wright, M.M. Babu, Classification of intrinsically disordered regions and proteins, Chem. Rev. 114 (2014) 6589–6631.
[22] P. Radivojac, L.M. Iakoucheva, C.J. Oldfield, Z. Obradovic, V.N. Uversky, A.K. Dunker, Intrinsic disorder and functional proteomics, Biophys. J. 92 (2007) 1439–1456.
[23] M.O. Collins, L. Yu, I. Campuzano, S.G. Grant, J.S. Choudhary, Phosphoproteomic analysis of the mouse brain cytosol reveals a predominance of protein phosphorylation in regions of intrinsic sequence disorder, Mol. Cell. Proteomics 7 (2008) 1331–1348.
[24] L.M. Iakoucheva, P. Radivojac, C.J. Brown, T.R. O'Connor, J.G. Sikes, Z. Obradovic, A.K. Dunker, The importance of intrinsic disorder for protein phosphorylation, Nucleic Acids Res. 32 (2004) 1037–1049.
[25] R. Dawson, L. Muller, A. Dehner, C. Klein, H. Kessler, J. Buchner, The N-terminal domain of p53 is natively unfolded, J. Mol. Biol. 332 (2003) 1131–1141.
[26] P.H. Kussie, S. Gorina, V. Marechal, B. Elenbaas, J. Moreau, A.J. Levine, N.P. Pavletich, Structure of the MDM2 oncoprotein bound to the p53 tumor suppressor transactivation domain, Science 274 (1996) 948–953.
[27] C.J. Oldfield, Y. Cheng, M.S. Cortese, P. Romero, V.N. Uversky, A.K. Dunker, Coupled folding and binding with alpha-helix-forming molecular recognition elements, Biochemistry 44 (2005) 12454–12470.
[28] M.G. Hinds, C. Smits, R. Fredericks-Short, J.M. Risk, M. Bailey, D.C. Huang, C.L. Day, Bim, Bad and Bmf: intrinsically unstructured BH3-only proteins that undergo a localized conformational change upon binding to prosurvival Bcl-2 targets, Cell Death Differ. 14 (2007) 128–136.
[29] G.J. Rautureau, C.L. Day, M.G. Hinds, Intrinsically disordered proteins in bcl-2 regulated apoptosis, Int. J. Mol. Sci. 11 (2010) 1808–1824.
[30] T. Dewpura, A. Raymond, J. Hamelin, N.G. Seidah, M. Mbikay, M. Chretien, J. Mayne, PCSK9 is phosphorylated by a Golgi casein kinase-like kinase ex vivo and circulates as a phosphoprotein in humans, FEBS J. 275 (2008) 3480–3493.
[31] V.S. Tagliabracci, S.E. Wiley, X. Guo, L.N. Kinch, E. Durrant, J. Wen, J. Xiao, J. Cui, K.B. Nguyen, J.L. Engel, J.J. Coon, N. Grishin, L.A. Pinna, D.J. Pagliarini, J.E. Dixon, A single kinase generates the majority of the secreted phosphoproteome, Cell 161 (2015) 1619–1632.
[32] S. Benjannet, D. Rhainds, R. Essalmani, J. Mayne, L. Wickham, W. Jin, M.C. Asselin, J. Hamelin, M. Varret, D. Allard, M. Trillard, M. Abifadel, A. Tebon, A.D. Attie, D.J. Rader, C. Boileau, L. Brissette, M. Chretien, A. Prat, N.G. Seidah, NARC-1/PCSK9 and its natural mutants: zymogen cleavage and effects on the low density lipoprotein (LDL) receptor and LDL cholesterol, J. Biol. Chem. 279 (2004) 48865–48875.
[33] S. Benjannet, D. Rhainds, J. Hamelin, N. Nassoury, N.G. Seidah, The proprotein convertase (PC) PCSK9 is inactivated by furin and/or PC5/6A: functional consequences of natural mutations and post-translational modifications, J. Biol. Chem. 281 (2006) 30561–30572.
[34] M. Abifadel, M. Guerin, S. Benjannet, J.P. Rabes, W. Le Goff, Z. Julia, J. Hamelin, V. Carreau, M. Varret, E. Bruckert, L. Tosolini, O. Meilhac, P. Couvert, D. Bonnefont-Rousselot, J. Chapman, A. Carrie, J.B. Michel, A. Prat, N.G. Seidah, C. Boileau, Identification and characterization of new gain-of-function mutations in the PCSK9 gene responsible for autosomal dominant hypercholesterolemia, Atherosclerosis 223 (2012) 394–400.
[35] K.E. Berge, L. Ose, T.P. Leren, Missense mutations in the PCSK9 gene are associated with hypocholesterolemia and possibly increased response to statin therapy, Arterioscler. Thromb. Vasc. Biol. 26 (2006) 1094–1100.
[36] C.W. Tsai, K.E. North, A. Tin, K. Haack, N. Franceschini, V. Saroja Voruganti, S. Laston, Y. Zhang, L.G. Best, J.W. MacCluer, T.H. Beaty, A. Navas-Acien, W.H. Kao, B.V. Howard, Both rare and common variants in PCSK9 influence plasma low-density lipoprotein cholesterol level in American Indians, J. Clin. Endocrinol. Metab. 100 (2015) E345–E349.
[37] S. Benjannet, Y.G. Saavedra, J. Hamelin, M.C. Asselin, R. Essalmani, A. Pasquato, P. Lemaire, G. Duke, B. Miao, F. Duclos, R. Parker, G. Mayer, N.G. Seidah, Effects of the prosegment and pH on the activity of PCSK9: evidence for additional processing events, J. Biol. Chem. 285 (2010) 40965–40978.
[38] J. Cameron, O.L. Holla, T. Ranheim, M.A. Kulseth, K.E. Berge, T.P. Leren, Effect of mutations in the PCSK9 gene on the cell surface LDL receptors, Hum. Mol. Genet. 15 (2006) 1551–1558.
[39] T.S. Fisher, P. Lo Surdo, S. Pandit, M. Mattu, J.C. Santoro, D. Wisniewski, R.T. Cummings, A. Calzetta, R.M. Cubbon, P.A. Fischer, A. Tarachandani, R. De Francesco, S.D. Wright, C. P. Sparrow, A. Carfi, A. Sitlani, Effects of pH and low density lipoprotein (LDL) on PCSK9-dependent LDL receptor regulation, J. Biol. Chem. 282 (2007) 20502–20512.
[40] Z. Zhao, Y. Tuakli-Wosornu, T.A. Lagace, L. Kinch, N.V. Grishin, J.D. Horton, J.C. Cohen, H.H. Hobbs, Molecular characterization of loss-of-function mutations in PCSK9 and identification of a compound heterozygote, Am. J. Hum. Genet. 79 (2006) 514–523.
[41] Y. Miyake, R. Kimura, Y. Kokubo, A. Okayama, H. Tomoike, T. Yamamura, T. Miyata, Genetic variants in PCSK9 in the Japanese population: rare genetic variants in PCSK9 might collectively contribute to plasma LDL cholesterol levels in the general population, Atherosclerosis 196 (2008) 29–36.
[42] T. Tajima, H. Morita, K. Ito, T. Yamazaki, M. Kubo, I. Komuro, Y. Momozawa, Blood lipid-related low-frequency variants in LDLR and PCSK9 are associated with onset age and risk of myocardial infarction in Japanese, Sci. Rep. 8 (2018) 8107.
[43] H. Mabuchi, A. Nohara, Therapy: PCSK9 inhibitors for treating familial hypercholesterolaemia, Nat. Rev. Endocrinol. 11 (2015) 8–9.
[44] T. Noguchi, S. Katsuda, M.A. Kawashiri, H. Tada, A. Nohara, A. Inazu, M. Yamagishi, J. Kobayashi, H. Mabuchi, The E32K variant of PCSK9 exacerbates the phenotype of familial hypercholesterolaemia by increasing PCSK9 function and concentration in the circulation, Atherosclerosis 210 (2010) 166–172.
[45] T. Kosenko, M. Golder, G. Leblond, W. Weng, T.A. Lagace, Low density lipoprotein binds to proprotein convertase subtilisin/kexin type-9 (PCSK9) in human plasma and inhibits PCSK9-mediated low density lipoprotein receptor degradation, J. Biol. Chem. 288 (2013) 8279–8288.
[46] O.L. Holla, J.K. Laerdahl, T.B. Strom, K. Tveten, J. Cameron, K.E. Berge, T.P. Leren, Removal of acidic residues of the prodomain of PCSK9 increases its activity towards the LDL receptor, Biochem. Biophys. Res. Commun. 406 (2011) 234–238.

[47] S. Mysling, K.K. Kristensen, M. Larsson, A.P. Beigneux, H. Gardsvoll, L.G. Fong, A. Bensadouen, T.J. Jorgensen, S.G. Young, M. Ploug, The acidic domain of the endothelial membrane protein GPIHBP1 stabilizes lipoprotein lipase activity by preventing unfolding of its catalytic domain, elife 5 (2016), e12095. .
[48] M.T. Lipari, W. Li, P. Moran, M. Kong-Beltran, T. Sai, J. Lai, S.J. Lin, G. Kolumam, J. Zavala-Solorio, A. Izrael-Tomasevic, D. Arnott, J. Wang, A.S. Peterson, D. Kirchhofer, Furin-cleaved proprotein convertase subtilisin/kexin type 9 (PCSK9) is active and modulates low density lipoprotein receptor and serum cholesterol levels, J. Biol. Chem. 287 (2012) 43482–43491.
[49] B. North, A. Lehmann, R.L. Dunbrack Jr., A new clustering of antibody CDR loop conformations, J. Mol. Biol. 406 (2011) 228–256.
[50] D.S. Wishart, B.D. Sykes, F.M. Richards, Relationship between nuclear magnetic resonance chemical shift and protein secondary structure, J. Mol. Biol. 222 (1991) 311–333.
[51] D.W. Buchan, F. Minneci, T.C. Nugent, K. Bryson, D.T. Jones, Scalable web services for the PSIPRED protein analysis workbench, Nucleic Acids Res. 41 (2013) W349–W357.
[52] D.T. Jones, Protein secondary structure prediction based on position-specific scoring matrices, J. Mol. Biol. 292 (1999) 195–202.
[53] F.M. Disfani, W.L. Hsu, M.J. Mizianty, C.J. Oldfield, B. Xue, A.K. Dunker, V.N. Uversky, L. Kurgan, MoRFpred, a computational tool for sequence-based prediction and characterization of short disorder-to-order transitioning binding regions in proteins, Bioinformatics 28 (2012) i75–i83.
[54] Y. Zhang, M. Ultsch, N.J. Skelton, D.J. Burdick, M.H. Beresini, W. Li, M. Kong-Beltran, A. Peterson, J. Quinn, C. Chiu, Y. Wu, S. Shia, P. Moran, P. Di Lello, C. Eigenbrot, D. Kirchhofer, Discovery of a cryptic peptide-binding site on PCSK9 and design of antagonists, Nat. Struct. Mol. Biol. 24 (2017) 848–856.
[55] V. Vacic, C.J. Oldfield, A. Mohan, P. Radivojac, M.S. Cortese, V.N. Uversky, A.K. Dunker, Characterization of molecular recognition features, MoRFs, and their binding partners, J. Proteome Res. 6 (2007) 2351–2366.
[56] A. Canales, M. Rosinger, J. Sastre, I.C. Felli, J. Jimenez-Barbero, G. Gimenez-Gallego, C. Fernandez-Tornero, Hidden alpha-helical propensity segments within disordered regions of the transcriptional activator CHOP, PLoS One 12 (2017), e0189171. .
[57] Y.S. Yang, C.C. Wang, B.H. Chen, Y.H. Hou, K.S. Hung, Y.C. Mao, Tyrosine sulfation as a protein post-translational modification, Molecules 20 (2015) 2138–2164.
[58] E.G. Cormier, M. Persuh, D.A. Thompson, S.W. Lin, T.P. Sakmar, W.C. Olson, T. Dragic, Specific interaction of CCR5 amino-terminal domain peptides containing sulfotyrosines with HIV-1 envelope glycoprotein gp120, Proc. Natl. Acad. Sci. U. S. A. 97 (2000) 5762–5767.
[59] M. Farzan, T. Mirzabekov, P. Kolchinsky, R. Wyatt, M. Cayabyab, N.P. Gerard, C. Gerard, J. Sodroski, H. Choe, Tyrosine sulfation of the amino terminus of CCR5 facilitates HIV-1 entry, Cell 96 (1999) 667–676.
[60] C.C. Huang, S.N. Lam, P. Acharya, M. Tang, S.H. Xiang, S.S. Hussan, R.L. Stanfield, J. Robinson, J. Sodroski, I.A. Wilson, R. Wyatt, C.A. Bewley, P.D. Kwong, Structures of the CCR5 N terminus and of a tyrosine-sulfated antibody with HIV-1 gp120 and CD4, Science 317 (2007) 1930–1934.
[61] E. Schnur, E. Noah, I. Ayzenshtat, H. Sargsyan, T. Inui, F.X. Ding, B. Arshava, Y. Sagi, N. Kessler, R. Levy, T. Scherf, F. Naider, J. Anglister, The conformation and orientation of a 27-residue CCR5 peptide in a ternary complex with HIV-1 gp120 and a CD4-mimic peptide, J. Mol. Biol. 410 (2011) 778–797.
[62] Z. Otwinowski, W. Minor, Processing of X-ray diffraction data collected in oscillation mode, Methods Enzymol. 276 (1997) 307–326.
[63] B. Webb, A. Sali, Comparative protein structure modeling using MODELLER, Curr. Protoc. Bioinformatics 47 (5 6) (2014) 1–32.
[64] P. Emsley, B. Lohkamp, W.G. Scott, K. Cowtan, Features and development of Coot, Acta Crystallogr. D Biol. Crystallogr. 66 (2010) 486–501.
[65] G.N. Murshudov, P. Skubak, A.A. Lebedev, N.S. Pannu, R.A. Steiner, R.A. Nicholls, M.D. Winn, F. Long, A.A. Vagin, REFMAC5 for the refinement of macromolecular crystal structures, Acta Crystallogr. D Biol. Crystallogr. 67 (2011) 355–367.
[66] G. Bricogne, E. Blanc, M. Brandl, C. Flensburg, P. Keller, W. Paciorek, P. Roversi, A. Sharff, O.S. Smart, C. Vonrhein, T.O. Womack, BUSTER version 2.11.2, Global Phasing Ltd., Cambridge, United Kingdom, 2011.
[67] P.D. Adams, P.V. Afonine, G. Bunkoczi, V.B. Chen, I.W. Davis, N. Echols, J.J. Headd, L.W. Hung, G.J. Kapral, R.W. Grosse-Kunstleve, A.J. McCoy, N.W. Moriarty, R. Oeffner, R.J. Read, D.C. Richardson, J.S. Richardson, T.C. Terwilliger, P.H. Zwart, PHENIX: a comprehensive Python-based system for macromolecular structure solution, Acta Crystallogr. D Biol. Crystallogr. 66 (2010) 213–221.
[68] R.L. Shields, A.K. Namenuk, K. Hong, Y.G. Meng, J. Rae, J. Briggs, D. Xie, J. Lai, A. Stadlen, B. Li, J.A. Fox, L.G. Presta, High resolution mapping of the binding site on human IgG1 for Fc gamma RI, Fc gamma RII, Fc gamma RIII, and FcRn and design of IgG1 variants with improved binding to the Fc gamma R, J. Biol. Chem. 276 (2001) 6591–6604.
[69] F. Delaglio, S. Grzesiek, G.W. Vuister, G. Zhu, J. Pfeifer, A. Bax, NMRPipe: a multidimensional spectral processing system based on UNIX pipes, J. Biomol. NMR 6 (1995) 277–293.
[70] B.A. Johnson, R.A. Blevins, NMR View: a computer program for the visualization and analysis of NMR data, J. Biomol. NMR 4 (1994) 603–614.
[71] Y. Wu, C. Eigenbrot, W.C. Liang, S. Stawicki, S. Shia, B. Fan, R. Ganesan, M.T. Lipari, D. Kirchhofer, Structural insight into distinct mechanisms of protease inhibition by antibodies, Proc. Natl. Acad. Sci. U. S. A. 104 (2007) 19784–19789.
[72] T. Yamamoto, C. Lu, R.O. Ryan, A two-step binding model of PCSK9 interaction with the low density lipoprotein receptor, J. Biol. Chem. 286 (2011) 5464–5470.
[73] M. Canuel, X. Sun, M.C. Asselin, E. Paramithiotis, A. Prat, N.G. Seidah, Proprotein convertase subtilisin/kexin type 9 (PCSK9) can mediate degradation of the low density lipoprotein receptor-related protein 1 (LRP-1), PLoS One 8 (2013), e64145. .
[74] M. Liu, G. Wu, J. Baysarowich, M. Kavana, G.H. Addona, K.K. Bierilo, J.S. Mudgett, G. Pavlovic, A. Sitlani, J.J. Renger, B.K. Hubbard, T.S. Fisher, C.V. Zerbinatti, PCSK9 is not involved in the degradation of LDL receptors and BACE1 in the adult mouse brain, J. Lipid Res. 51 (2010) 2611–2618.
[75] S. Poirier, G. Mayer, S. Benjannet, E. Bergeron, J. Marcinkiewicz, N. Nassoury, H. Mayer, J. Nimpf, A. Prat, N.G. Seidah, The proprotein convertase PCSK9 induces the degradation of low density lipoprotein receptor (LDLR) and its closest family members VLDLR and ApoER2, J. Biol. Chem. 283 (2008) 2363–2372.

[76] A. Roubtsova, M.N. Munkonda, Z. Awan, J. Marcinkiewicz, A. Chamberland, C. Lazure, K. Cianflone, N.G. Seidah, A. Prat, Circulating proprotein convertase subtilisin/kexin 9 (PCSK9) regulates VLDLR protein and triglyceride accumulation in visceral adipose tissue, Arterioscler. Thromb. Vasc. Biol. 31 (2011) 785–791.

[77] L. Shan, L. Pang, R. Zhang, N.J. Murgolo, H. Lan, J.A. Hedrick, PCSK9 binds to multiple receptors and can be functionally inhibited by an EGF-A peptide, Biochem. Biophys. Res. Commun. 375 (2008) 69–73.

[78] H.M. Gu, A. Adijiang, M. Mah, D.W. Zhang, Characterization of the role of EGF-A of low density lipoprotein receptor in PCSK9 binding, J. Lipid Res. 54 (2013) 3345–3357.

[79] R. Essalmani, D. Susan-Resiga, A. Chamberland, M. Abifadel, J.W. Creemers, C. Boileau, N.G. Seidah, A. Prat, In vivo evidence that furin from hepatocytes inactivates PCSK9, J. Biol. Chem. 286 (2011) 4257–4263.

[80] B. Han, P.I. Eacho, M.D. Knierman, J.S. Troutt, R.J. Konrad, X. Yu, K.M. Schroeder, Isolation and characterization of the circulating truncated form of PCSK9, J. Lipid Res. 55 (2014) 1505–1514.

[81] K. Tveten, O.L. Holla, J. Cameron, T.B. Strom, K.E. Berge, J.K. Laerdahl, T.P. Leren, Interaction between the ligand-binding domain of the LDL receptor and the C-terminal domain of PCSK9 is required for PCSK9 to remain bound to the LDL receptor during endosomal acidification, Hum. Mol. Genet. 21 (2012) 1402–1409.

[82] D.E. Piper, S. Jackson, Q. Liu, W.G. Romanow, S. Shetterly, S.T. Thibault, B. Shan, N.P. Walker, The crystal structure of PCSK9: a regulator of plasma LDL-cholesterol, Structure 15 (2007) 545–552.